

Upscale Feedback of Tropical Synoptic Variability to Intraseasonal Oscillations through the Nonlinear Rectification of the Surface Latent Heat Flux*

CHUNHUA ZHOU⁺ AND TIM LI

Department of Meteorology, University of Hawaii at Manoa, Honolulu, Hawaii

(Manuscript received 7 October 2009, in final form 15 April 2010)

ABSTRACT

Analysis of observational data suggests two-way interactions between the tropical intraseasonal oscillation (ISO) and synoptic-scale variability (SSV). On one hand, SSV is strongly modulated by the ISO; that is, a strengthened (weakened) SSV appears during the enhanced (suppressed) ISO phase. The northwest-southeast-oriented synoptic wave train is strengthened and well organized in the northwestern Pacific during the enhanced ISO phase but weakened during the suppressed ISO phase. On the other hand, SSV may exert an upscale feedback to ISO through the nonlinearly rectified surface latent heat flux (LHF). The maximum synoptic contribution exceeds 20%–30% of the total intraseasonal LHF over the tropical Indian Ocean, western Pacific, and northeastern Pacific. The nonlinearly rectified LHF leads the ISO convection and boundary layer specific humidity, and thus it may contribute to the propagation of the ISO in boreal summer through the preconditioning of the surface moisture and moist static energy ahead of the convection.

1. Introduction

The intraseasonal oscillation (ISO), or the Madden-Julian oscillation (MJO; Madden and Julian 1971, 1972), is the most significant subseasonal signal in the tropical atmosphere [see Zhang (2005) for a review]. It has great regional and season-dependent evolution characteristics (Rui and Wang 1990; Madden and Julian 1994). It is well connected to the monsoon intraseasonal variability in boreal summer through the northward propagation of the ISO convection (Yasunari 1979; Jiang et al. 2004). The ISO behaves differently during the developing and decaying phases of ENSO (Lin and Li 2008; Seiki et al. 2009; Roundy and Kravitz 2009).

The tropical Indian Ocean and western Pacific are regions of enhanced ISOs and synoptic-scale variabilities (SSVs), including tropical cyclone (TC) activity (Lau and

Lau 1990; Liebmann et al. 1994; Hartmann and Maloney 2001; Li et al. 2003; Maloney and Dickinson 2003; Straub and Kiladis 2003; Fu et al. 2007). It is well known that the ISO may exert a large-scale control on SSVs (Liebmann et al. 1994; Hendon and Liebmann 1994; Maloney and Hartmann 1998, 2000a,b; Straub and Kiladis 2003). Nakazawa (1988) showed that synoptic-scale disturbances are embedded within “super clusters” during the enhanced (or convective) phase of the ISO. Diagnostic and modeling studies suggest that barotropic energy conversion between the intraseasonal flow field and higher-frequency eddies is responsible for the latter’s growth (Maloney and Hartmann 2001; Hartmann and Maloney 2001; Sobel and Maloney 2000; Maloney and Dickinson 2003). A case study by Dickinson and Molinari (2002) pointed out an association between the mixed Rossby-gravity wave packet-TC activity and the enhanced convective phase of the MJO.

Studies have pointed out relationships between the occurrence of TCs and the ISO (Liebmann et al. 1994). Maloney and Hartmann (1998, 2000a) calculated correlations between the enhanced phase of MJO and TC genesis and suggested that the MJO westerly phase may set up favorable conditions for TC development by inducing cyclonic low-level vorticity and boundary layer convergences. Using wave accumulation as a precondition for TC genesis, Sobel and Maloney (2000) found

* School of Ocean and Earth Science and Technology Contribution Number 7932 and International Pacific Research Center Contribution Number 693.

⁺ Current affiliation: Research Applications Laboratory, National Center for Atmospheric Research, Boulder, Colorado.

Corresponding author address: Chunhua Zhou, RAL, NCAR, 3450 Mitchell Lane, Boulder, CO 80301.
E-mail: chunhua@ucar.edu

that the wave activity convergence associated with tropical-depression-type disturbances is stronger during the enhanced phase of the MJO. Frank and Roundy (2006) found that tropical cyclone formation is closely related to enhanced tropical wave activity, including the mixed Rossby-gravity waves, tropical-depression-type or easterly waves, equatorial Rossby waves, and the MJO.

Yet, compared with the ISO control on synoptic-scale activity, the SSV feedback to the ISO has received less attention (Batstone et al. 2005). Many of the previous studies emphasized the ISO influence on SSV, and less attention was paid to the synoptic feedback to the ISO. While the ISO exerts a large-scale control on SSV, it is not clear how and to what extent the integrated effect of SSVs and TCs may further feed back to the ISO by changing its strength, structure, and propagation characteristics. Krishnamurti et al. (2003) speculated that about 30%–50% of the total surface heat flux on the MJO time scale might come from the interaction of the MJO with other time scales. It has been suggested that the synoptic-scale motion may trigger the MJO (Biello and Majda 2005; Biello et al. 2007). A significant reduction of ISO variances was found when removing TCs from the National Centers for Environmental Prediction (NCEP) reanalysis data (Hsu et al. 2008), suggesting a two-way interaction between TCs and the ISO.

This study is to examine the two-way interaction between the tropical ISO and SSV, including the modulation of the ISO on SSV and the SSV feedback to the ISO. The rest of this paper is organized as follows. Data and analysis methods are described in section 2, followed by an analysis of the ISO modulation on SSV in section 3. Section 4 diagnoses the SSV contribution to the intraseasonal latent heat flux and its phase relationship with the ISO convection. A summary is given in section 5.

2. Data and methods

The primary data used in this study include 1) daily National Oceanic and Atmospheric Administration (NOAA) interpolated outgoing longwave radiation (OLR) at a grid of $2.5^\circ \times 2.5^\circ$ for 1979–2006; 2) NCEP/Department of Energy (DOE) Global Reanalysis 2 (NCEP-2) data provided by NOAA's Oceanic and Atmospheric Research (OAR), Earth System Research Laboratory (ESRL), Physical Sciences Division (PSD) in Boulder, Colorado (available online at <http://www.cdc.noaa.gov/>, 4 times daily data for 1979–2008); 3) European Centre for Medium-Range Weather Forecasts (ECMWF) Tropical Ocean and Global Atmosphere (TOGA) Global Advanced Operational Surface Analysis (4 times daily for 1986–2006); 4) 3-day running mean Tropical Rainfall Measuring Mission (TRMM) Microwave Imager (TMI) Sea Surface

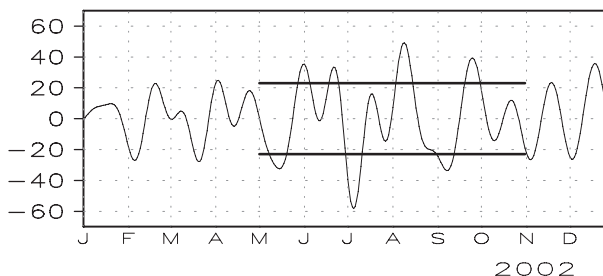


FIG. 1. Box-averaged (15° – 20° N, 125° – 135° E) 20–90-day filtered OLR in 2002. The horizontal axis is the month of the year and the vertical axis is the amplitude of the OLR (W m^{-2}). The thick solid lines represent a positive and a negative one standard deviation in the summer period (May–October).

Temperature (SST; version 4, daily, on a grid of $0.25^\circ \times 0.25^\circ$ for 1998–2006); and 5) Woods Hole Oceanographic Institution (WHOI) objectively analyzed air–sea fluxes (OAFflux; daily, on a grid of $1^\circ \times 1^\circ$ for 1981–2002; Yu and Weller 2007).

The surface latent heat flux (LHF) from the WHOI OAFflux dataset is used to validate the bulk formula calculation. To accommodate the 6-hourly NCEP-2 and ECMWF TOGA Global Advanced Operational Surface Analysis data for the LHF calculation, the daily TMI SST is interpolated to 4 times daily.

Treating the OLR field as a proxy for tropical convection, we define the enhanced and suppressed phases of the ISO based on the 20–90-day bandpass-filtered daily OLR data. Note that the ISO referred to here may include the MJO, equatorial Rossby waves, and other tropical waves. A multivariate empirical orthogonal function (MEOF) analysis is performed onto the 3–8-day filtered wind and vorticity fields to derive the leading modes of SSV during the enhanced and suppressed ISO phases, respectively. The difference between the regular EOF and the multivariate EOF is that the former is performed onto a single variable, while the latter works on a combination of several variables. For example, the leading MEOF modes of two variables give paired spatial patterns. Using one standard deviation of the time series of the first MEOF mode as a threshold, 16 (24) SSV cases are selected for a composite analysis to derive the evolution of dominant SSV patterns during the enhanced (suppressed) ISO phases.

3. Modulation of SSV by the ISO

A 20–90-day bandpass filter is applied to the OLR field for the summer period (May–October) of 2000–06 to isolate the ISO signal. A reference region (15° – 20° N, 125° – 135° E), where the strongest ISO variability appears in the western North Pacific (WNP), is selected. The

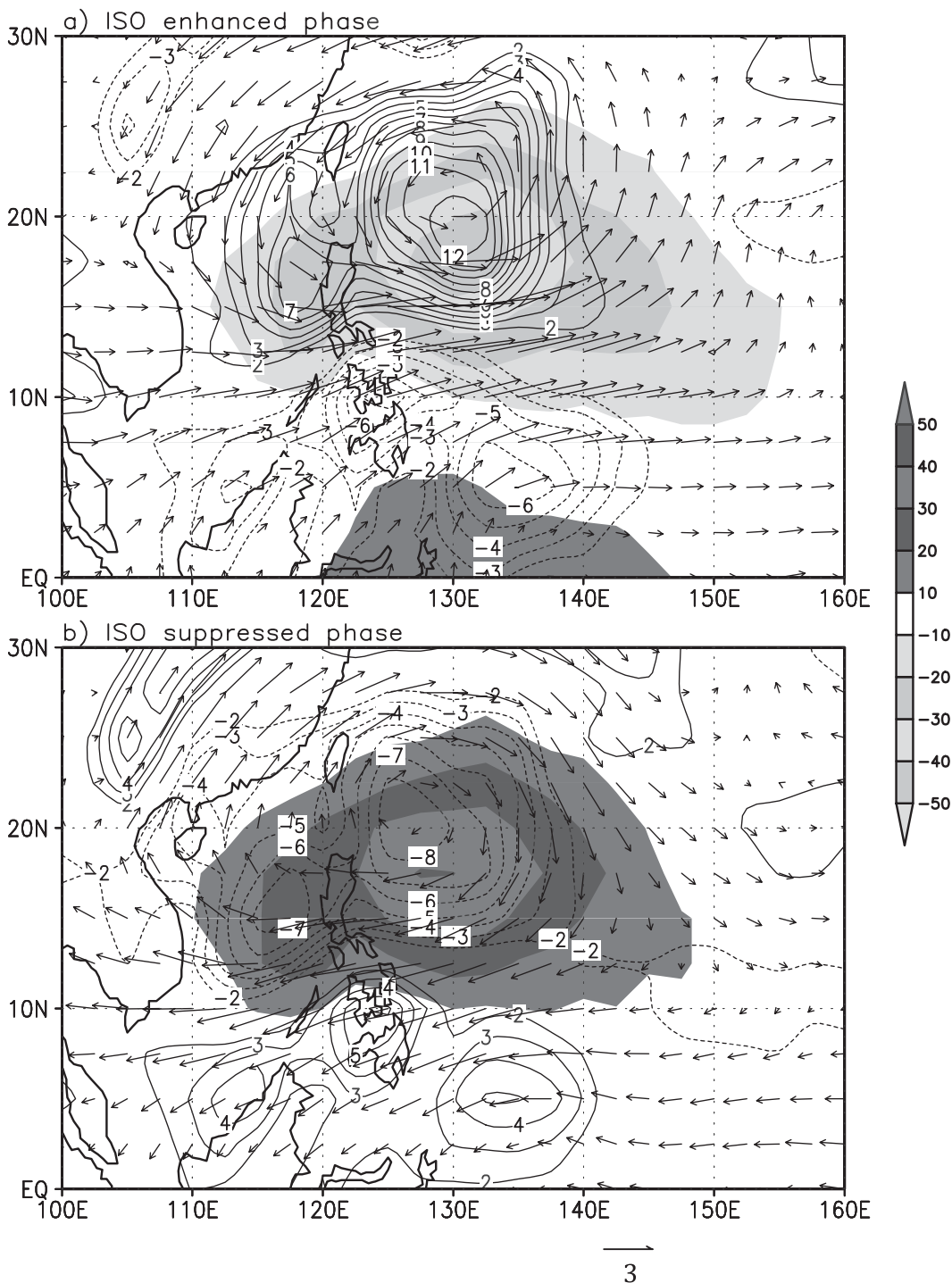


FIG. 2. The 20–90-day filtered OLR (shading, W m^{-2}), 850-mb vorticity (contour, 10^{-6} s^{-1}) and wind (vector, m s^{-1}) fields during the ISO (a) enhanced and (b) suppressed phases in the NWP in boreal summer (2000–06).

enhanced and suppressed ISO phases are then defined according to the reference-box-averaged filtered OLR field, with one standard deviation as a threshold. The time series of box-averaged OLR for year 2002 is shown

in Fig. 1 as an example, in which the solid line denotes one standard deviation in the summer period.

Figure 2 illustrates the spatial distribution of the 20–90-day filtered 850-hPa wind (vector), relative vorticity

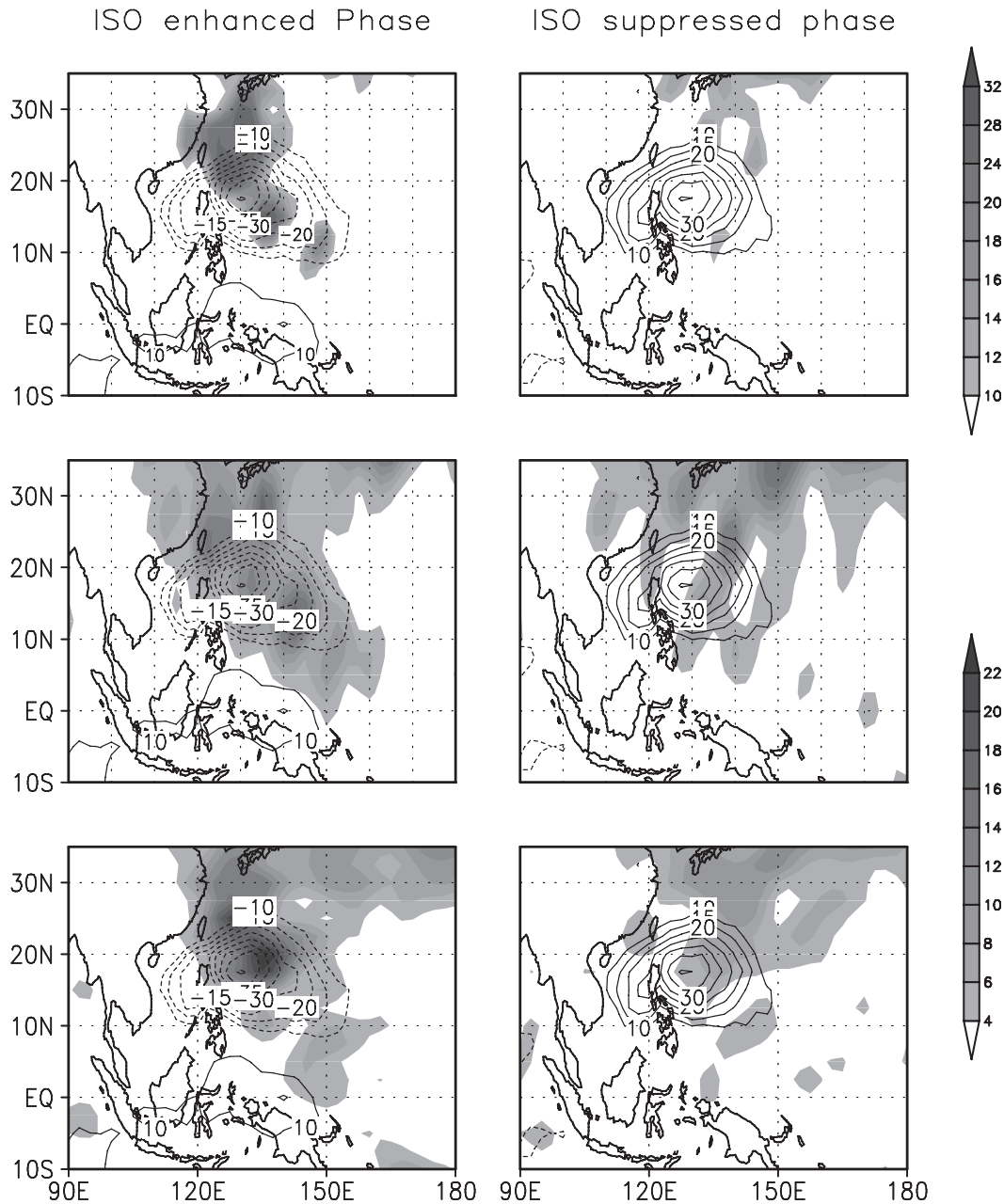


FIG. 3. Variances (shading) of the synoptic-scale (top) vorticity (10^{-11} s^{-2}), (middle) meridional wind ($\text{m}^2 \text{ s}^{-2}$), and (bottom) zonal wind ($\text{m}^2 \text{ s}^{-2}$) fields at 850 mb for the (left) enhanced and (right) suppressed ISO phases in the WNP. The contours are for the 20–90-day filtered OLR field (W m^{-2}).

(contour), and OLR (shading) fields during the enhanced and suppressed ISO phases. Note that the enhanced (suppressed) ISO convection is associated with low-level cyclonic (anticyclonic) circulation, with the vorticity centers located slightly northwest of the convection centers (Hsu and Weng 2001; Li and Wang 2005). The cause of this vorticity phase shift is attributed to the effect of both the background vertical shear (Jiang et al. 2004) and the planetary vorticity gradient.

Is the synoptic-scale motion randomly distributed or is it ISO phase dependent? To address this question, the synoptic-scale (3–8 days) variance is examined in the WNP for the enhanced and suppressed ISO phases. Figure 3 shows the variances of the synoptic-scale vorticity, zonal wind, and meridional wind at 850 hPa for the ISO enhanced and suppressed phases. A significant difference exists between the enhanced and suppressed ISO phases, with stronger (weaker) SSV occurring during the

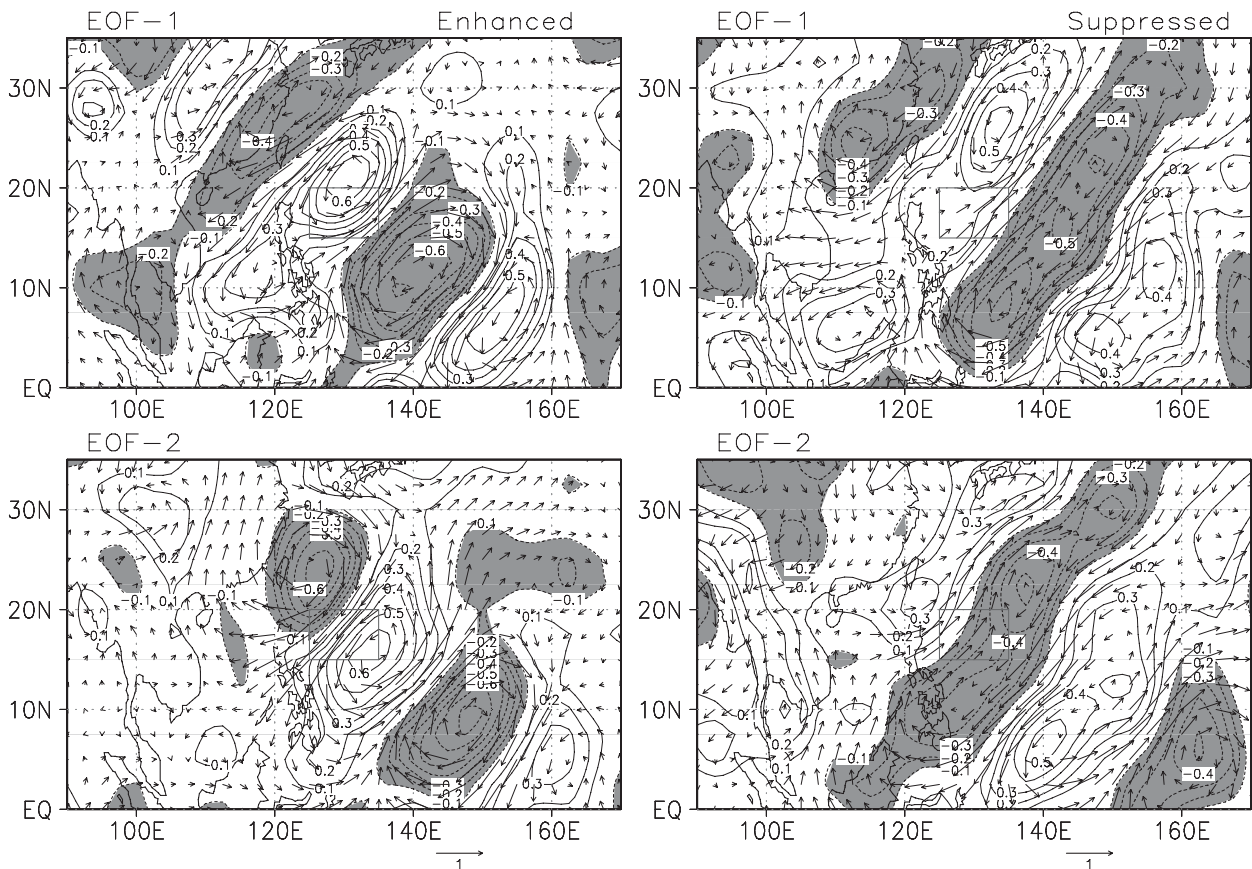


FIG. 4. (top) First and (bottom) second EOF modes of the 3–8-day filtered 850-mb wind (vectors) and vorticity (contours) fields during the ISO (left) enhanced and (right) suppressed phases in the NWP. The box represents the reference region (15° – 20° N, 125° – 135° E).

enhanced (suppressed) phase of ISO. The greatest differences appear at the center and to the north of the ISO convection. Other variables—such as the surface latent heat flux, humidity, and SST—also show similar characteristics, indicating that SSV is in general stronger (weaker) during the enhanced (suppressed) ISO phase.

To illustrate the spatial and temporal structures of the SSV, we conducted a multivariate EOF analysis of the synoptic-scale 850-hPa zonal wind and vorticity fields in the WNP domain (0° – 35° N, 90° – 170° E) for the enhanced and suppressed ISO phases, respectively. While the zonal wind alone might be sufficient to describe the boreal winter ISO (or MJO), the boreal summer ISO involves a greater rotational wind component and is characterized by marked northward and westward propagation. As the vorticity includes both the zonal and meridional wind components, both the zonal wind and vorticity fields are considered in our eigenmode calculation. Figure 4 shows horizontal patterns of the first and second EOF modes of SSV during the enhanced and suppressed ISO phases. Note that the dominant SSV pattern is a northwest–southeast-oriented synoptic-scale wave train, consistent

with previous studies (e.g., Lau and Lau 1990; Li 2006; Tam and Li 2006). By analyzing TC genesis events in the WNP during 2000/01, Fu et al. (2007) found that about 30% of cyclogenesis events occur in the synoptic wave train (excluding those due to the energy dispersion of a preexisting TC). Kiladis et al. (2009) found a similar wave train pattern that connects a mixed Rossby gravity wave to the east. The EOF-1 and EOF-2 patterns in Fig. 4 represent different phases of the same SSV mode that propagates northwestward.

To further reveal the structure and evolution characteristics of SSV, a composite analysis is performed for the enhanced and suppressed ISO phases, respectively, based on the EOF-1 time series. Figure 5 shows the evolution of the synoptic-scale wind and vorticity fields at 850 hPa from day -3 to day 2 for the enhanced phase of the ISO, where day 0 corresponds to the strongest SSV in the reference box. A well-organized alternative cyclone–anticyclone–cyclone wave train is found in the WNP, and the wave train propagates northwestward at a phase speed of about 3 m s^{-1} . The amplitude of the vorticity field exceeds $2 \times 10^{-5} \text{ s}^{-1}$.

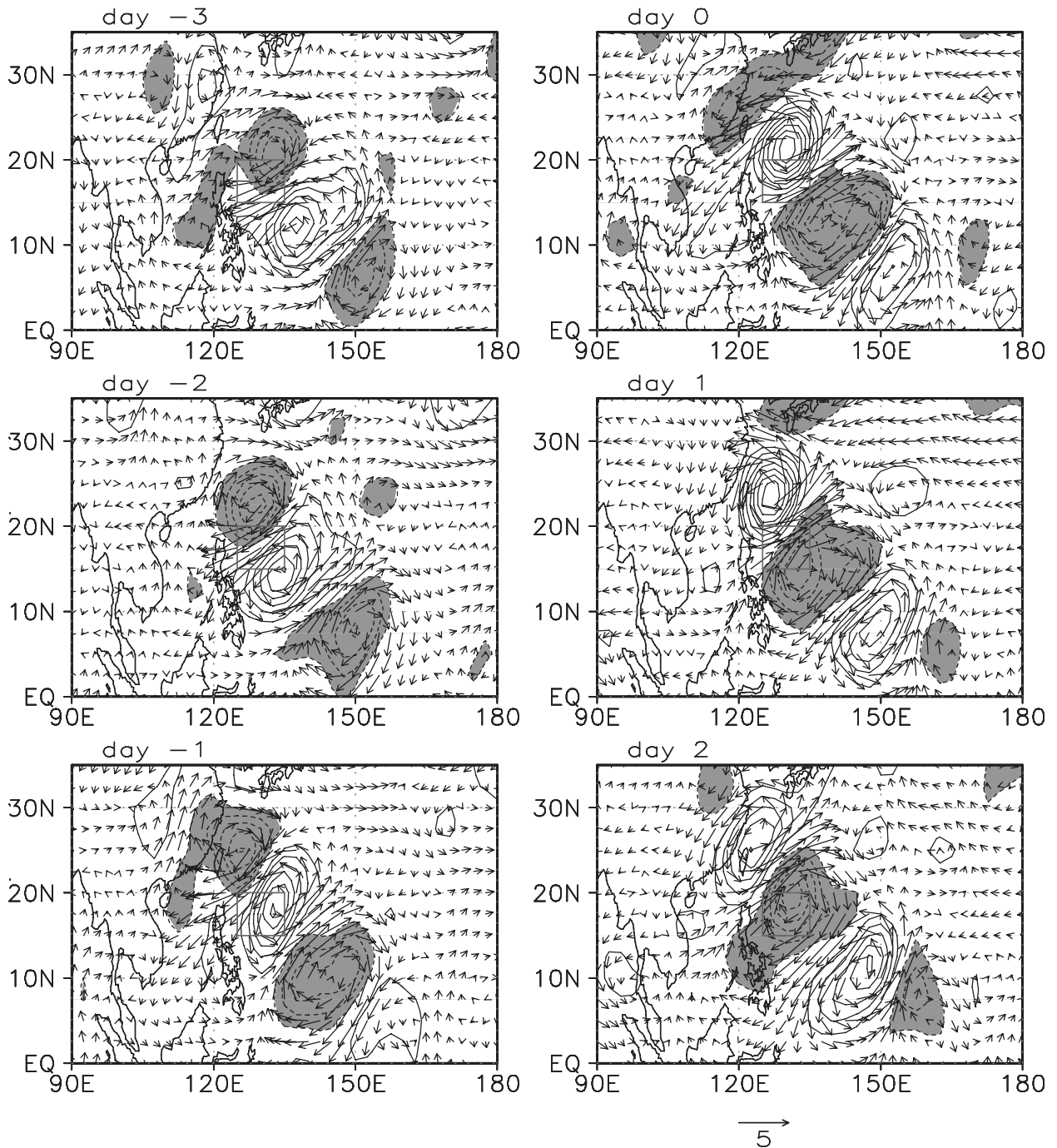


FIG. 5. Time evolution of the synoptic-scale wind (vector, m s^{-1}) and vorticity (contour, interval: $0.3 \times 10^{-5} \text{ s}^{-1}$) fields at 850 mb from day -3 to day 2 during the enhanced ISO phase. Day 0 corresponds to a time when the strongest synoptic disturbance appears in the reference box.

Figure 6 illustrates the corresponding SSV pattern and evolution during the suppressed phase of ISO. It is obvious that the wave train is much weaker and is loosely organized. The amplitude of the 850-hPa vorticity field is 3–4 times smaller. The propagation speed of the

synoptic-scale wave train during the suppressed phase is slower, about one-half of that during the enhanced ISO phase.

The distinct SSV patterns during the enhanced and suppressed ISO phases are consistent with previous studies.

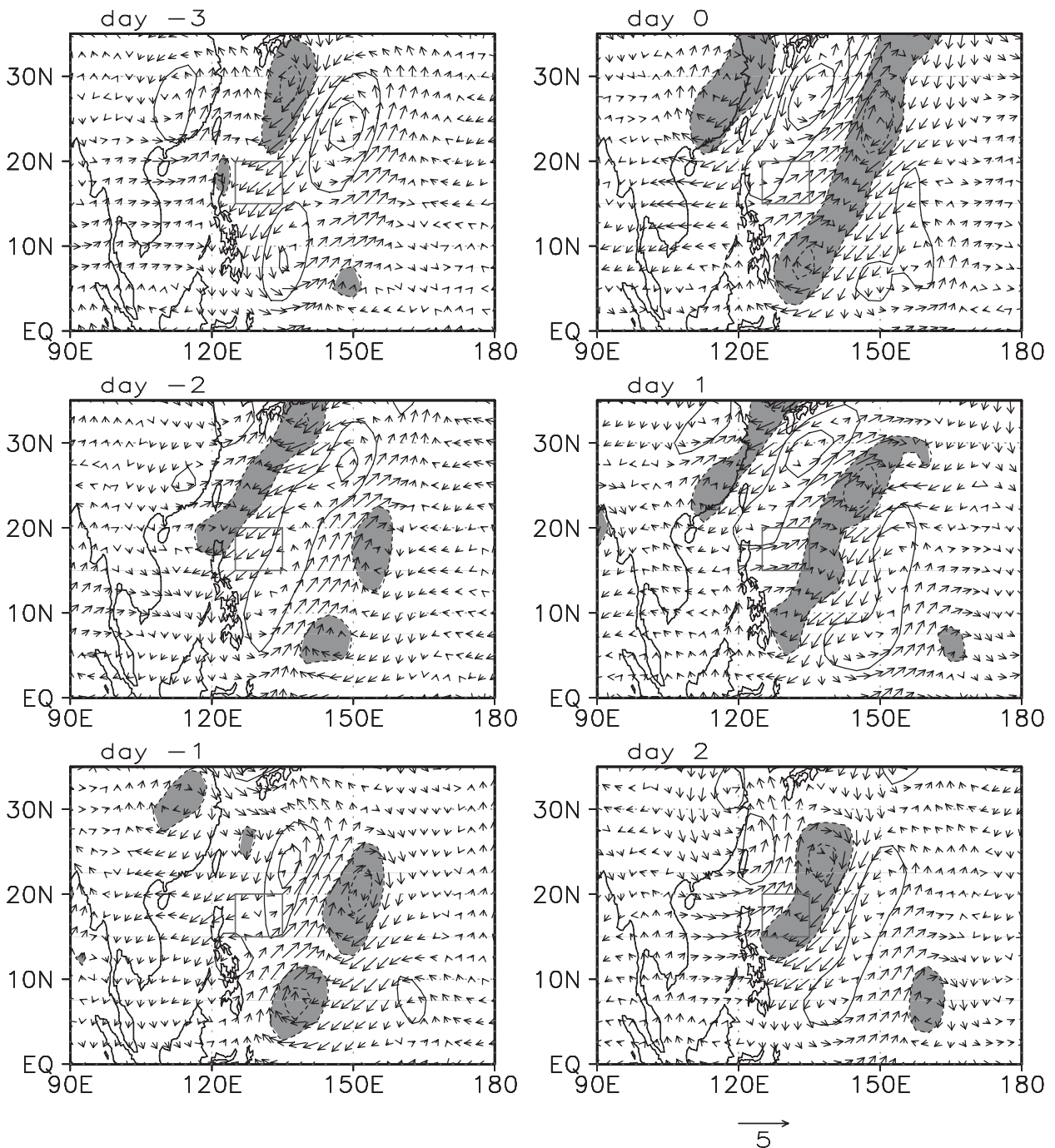


FIG. 6. As in Fig. 5, but for the suppressed ISO phase.

For example, Maloney and Dickinson (2003) showed that tropical-depression-type disturbances are more energetic during ISO westerly periods than during ISO easterly periods. Ko and Hsu (2009) also pointed out that the wave pattern is better organized in the ISO westerly phase.

Following the same method, one may reveal the evolution characteristics of the synoptic-scale SST and surface

specific humidity fields in relevance to the 850-hPa synoptic wind pattern (Figs. 7, 8). Note that positive (negative) synoptic SST perturbations appear slightly ahead of the cyclonic (anticyclonic) circulation. The magnitude of the SST anomalies during the enhanced ISO phase (0.25°C) is about twice of that during the suppressed ISO phase (about $0.1^{\circ}\text{--}0.15^{\circ}\text{C}$). Figure 8 shows

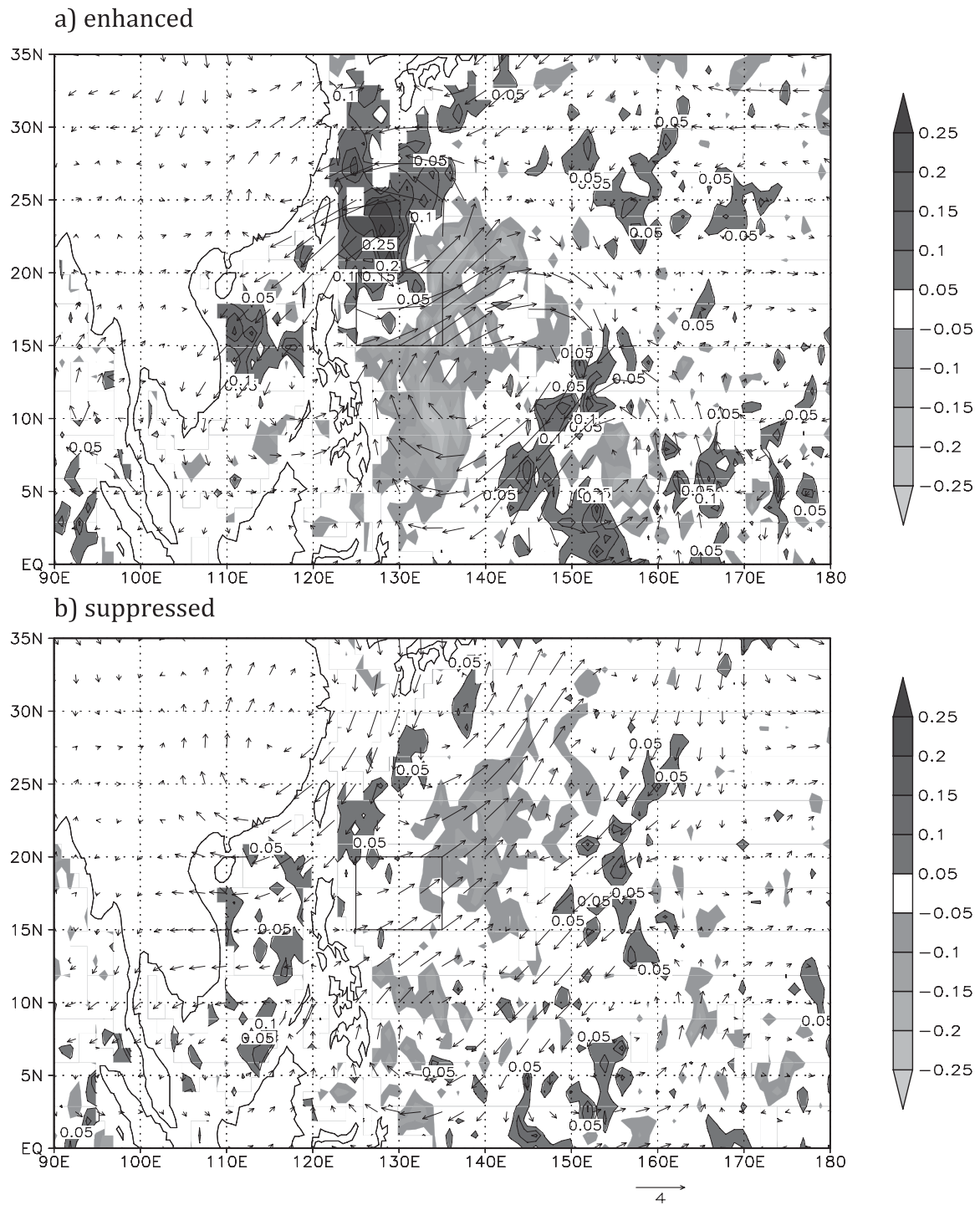


FIG. 7. Synoptic-scale SST (shading: negative SST; shading and contours: positive SST; unit: $^{\circ}\text{C}$) and 850-hPa wind (vector, m s^{-1}) fields at day 0 during the (a) enhanced and (b) suppressed ISO phases.

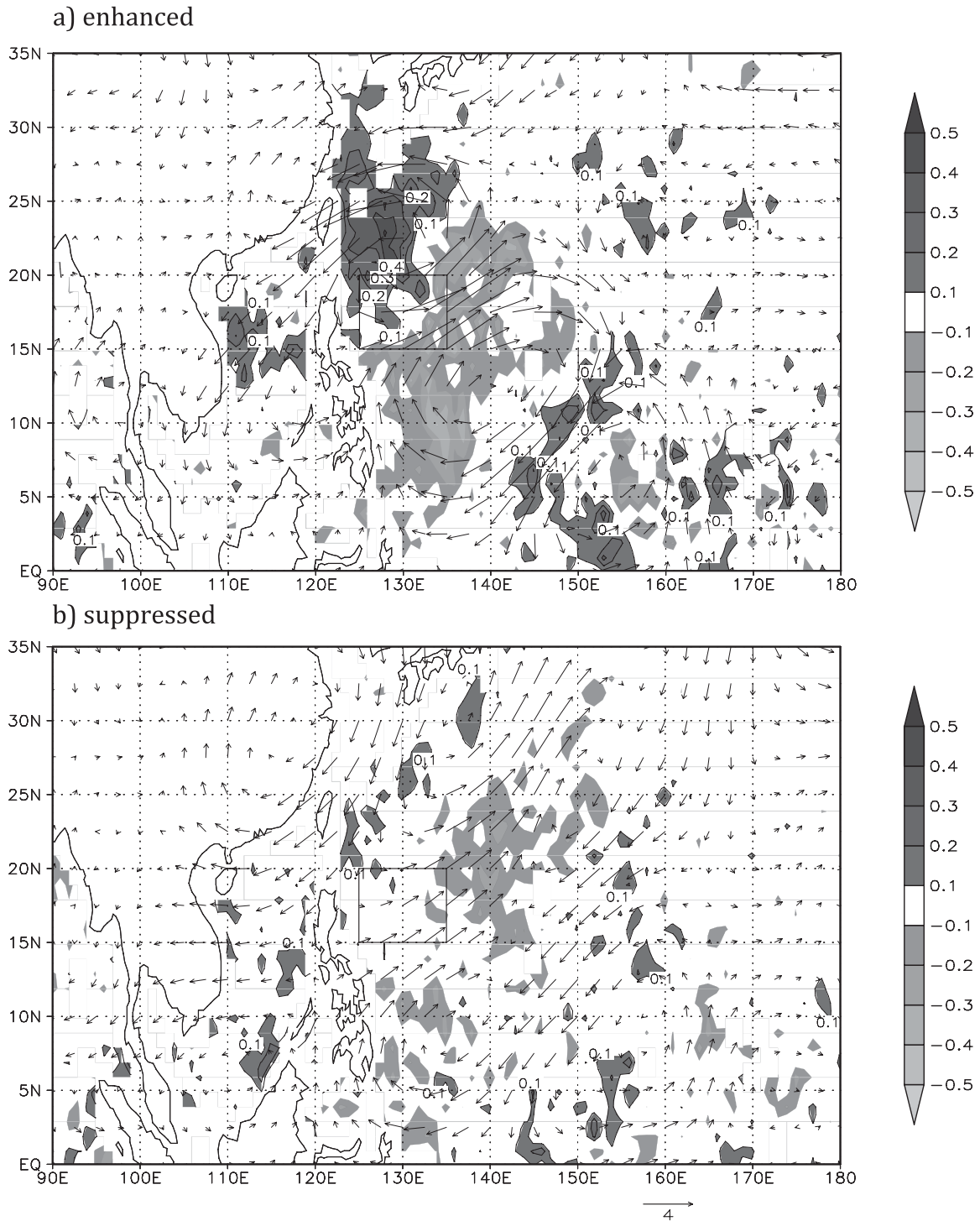


FIG. 8. As in Fig. 7, but for the synoptic-scale surface specific humidity field (shading: negative surface specific humidity; shading and contours: positive surface specific humidity; unit: g kg^{-1}).

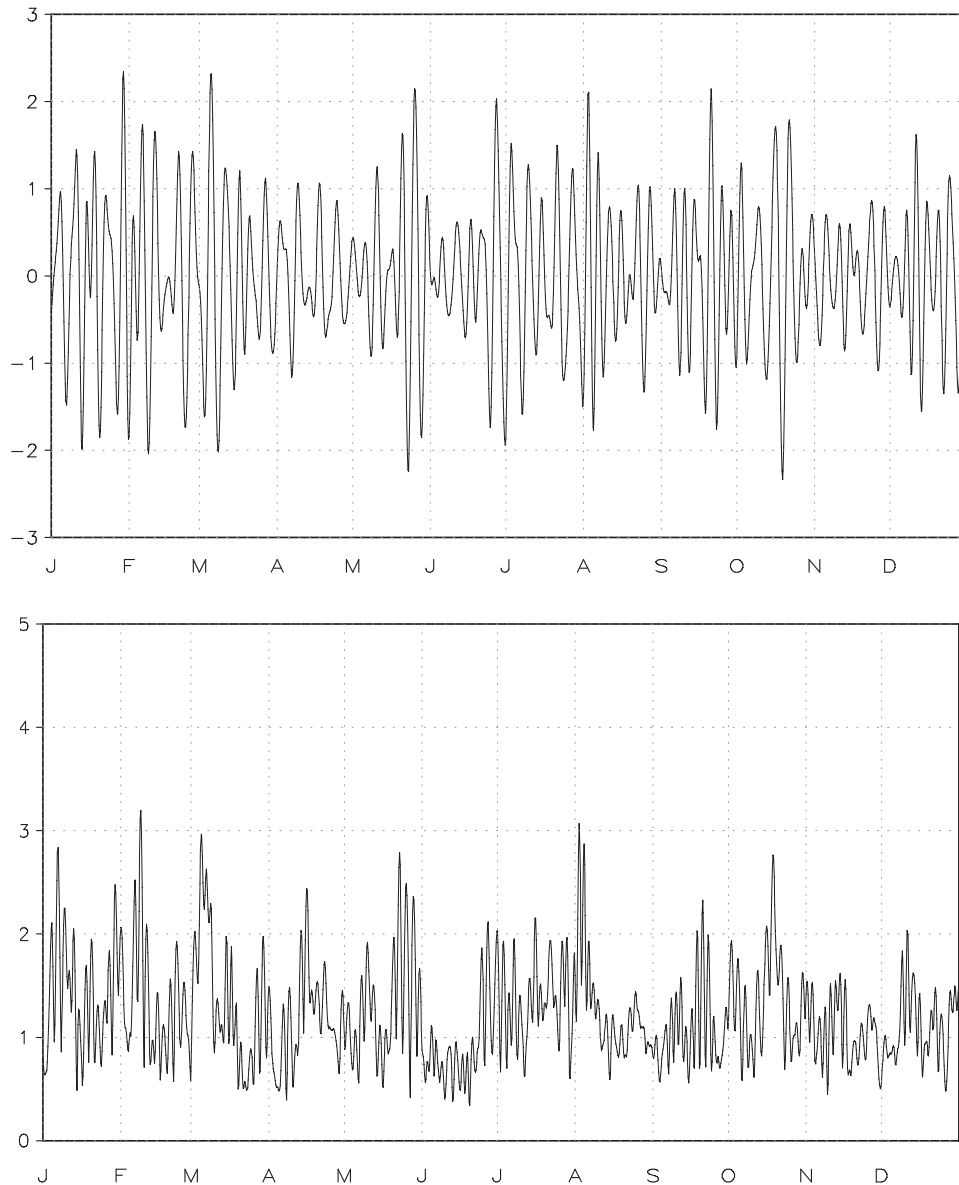


FIG. 9. Time series of the box-averaged (2.5°S – 2.5°N , 75° – 85°E) synoptic-scale (top) zonal wind and (bottom) wind speed at 10 m in 2001. The wind speed is calculated based on the 3–8-day filtered zonal and meridional wind components. The unit is m s^{-1} .

the structure of the synoptic-scale surface specific humidity derived from the ECMWF global analysis. For both the enhanced (upper panel) and suppressed (lower panel) phases of the ISO, positive (negative) synoptic-scale humidity perturbations also appear slightly ahead of the low-level cyclonic (anticyclonic) vorticity field, in accordance with the SST field. The amplitude of the specific humidity field during the enhanced ISO phase (0.4 g kg^{-1}) is about twice of that during the suppressed ISO phase (0.2 g kg^{-1}). The resemblance of the spatial pattern of the synoptic-scale SST and surface specific

humidity fields implies that the Lindzen and Nigam (1987) mechanism works on the synoptic scale—a warm SST perturbation leads to a PBL convergence and thus an increase of the surface humidity.

The observational evidences mentioned earlier show an in-phase relationship between the ISO and SSV; that is, a stronger (weaker) northwest–southeast-oriented wave train appears during the enhanced (suppressed) phase of the ISO. What causes such a phase dependence? A possible mechanism is attributed to the change of the background vertical shear (Ge et al. 2007). During the

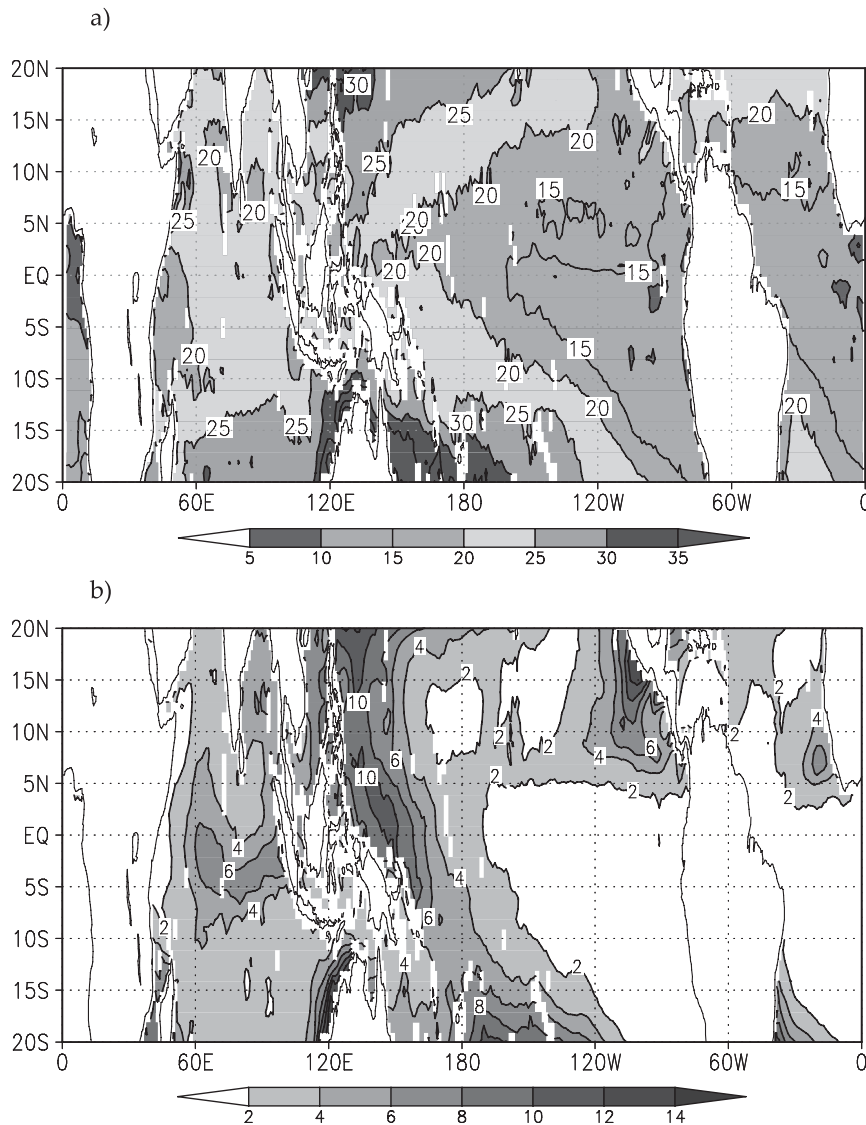


FIG. 10. Standard deviations of the 20–90-day filtered surface LHF calculated based on the bulk formula from the (a) total fields and (b) 3–8-day filtered and background mean fields. The contour interval is (top) 5 and (bottom) 2 W m^{-2} .

enhanced (suppressed) ISO phase, as convective heating in the WNP is strengthened (weakened), so is the easterly shear of the background zonal wind. Through a theoretical study, Wang and Xie (1996) indicated that under an easterly (westerly) shear, the amplitude of equatorial Rossby waves is enhanced (weakened) at the lower troposphere while weakened (enhanced) at the upper troposphere. Li (2006) further examined the asymmetric growth of the synoptic wave train in the WNP under a constant easterly and westerly shear and found that the wave train grows much faster under an easterly shear. Therefore, the enhanced easterly shear during the enhanced ISO phase might lead to the amplification of low-level vorticity,

which further enhances the PBL convergence (through the Ekman pumping) and convective heating, leading to the strong development of the synoptic disturbance.

4. Upscale feedback of SSV to the ISO

In this section, we focus on how the synoptic-scale motion may nonlinearly rectify the intraseasonal surface LHF and what is the phase relationship between the nonlinearly rectified LHF and the ISO convection. It is hypothesized that the SSV-rectified LHF may affect the ISO convection through the preconditioning of the surface moisture and moist static energy.

a. SSV contribution to the intraseasonal LHF

The surface LHF may be calculated according to the following bulk formula (Weare et al. 1981; Chu and Frederick 1990):

$$\text{LHF} = L\rho C_E |\mathbf{V}| (q_s - q_a), \quad (1)$$

where $L = 2.5 \times 10^6 \text{ J kg}^{-1}$ is the latent heat of condensation; $\rho = 1.225 \text{ kg m}^{-3}$ is the air density at the standard sea level; C_E is a constant exchange coefficient whose value is determined based on the comparison with the climatology annual cycle of OAFflux; $|\mathbf{V}|$ is 10-m wind speed based on the 6-hourly ECMWF data; q_s is the sea surface specific humidity derived from the 6-hourly interpolated TMI SST and 6-hourly sea level pressure (SLP) from the ECMWF TOGA analysis; and q_a is the specific humidity at 10 m, derived based on the 6-hourly SLP and dewpoint temperature from the ECMWF TOGA analysis.

A constant exchange coefficient of 1×10^{-3} is selected, based on a comparison with the annual cycle of the WHOI OAFflux for the period of 2000–02. Both the OAFflux and calculated LHF fields show large variances in northeastern Asia and relatively small variances over the tropical oceans. The resemblance of both the mean and variability patterns between the observed and calculated LHF datasets gives us the confidence to further use the bulk formula for the subsequent nonlinear rectification analysis.

There are two ways for SSV to nonlinearly rectify the intraseasonal LHF field. The first way is through the nonlinear rectification of the surface wind speed. Figure 9 shows an example illustrating how synoptic wind components may give rise to intraseasonal variation of the wind speed. Year 2001 was randomly chosen here, as each year bears a similar feature. Whereas the integrated values of 3–8-day filtered zonal wind (top panel in Fig. 9) and meridional wind over an intraseasonal or longer period are approximately zero, the derived wind speed (bottom panel in Fig. 9) exhibits a clear intraseasonal oscillation. This nonlinearly rectified wind speed may further contribute to the intraseasonal LHF variability. The second way is through the nonlinear interaction between the synoptic-scale air–sea humidity difference and motion.

To examine to what extent SSV contributes to the intraseasonal surface LHF, the zonal (u) and meridional (v) wind components and the air–sea humidity difference (Δq) fields are decomposed into three components: the climatological background mean state, the synoptic-scale (3–8 days) component, and the intraseasonal (20–90 day) component. Either the climatological annual

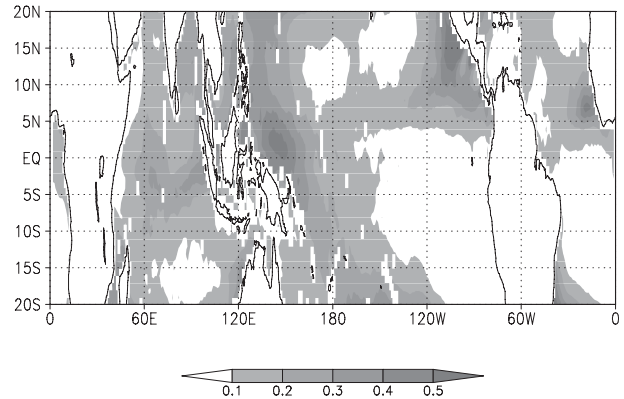


FIG. 11. Ratio of the standard deviations of the nonlinearly rectified intraseasonal surface LHF (calculated based on the 3–8-day filtered and background mean fields) to the total intraseasonal surface LHF.

mean or annual cycle field may be used to represent the background state. For simplicity, an annual mean state is used in this study.

Two intraseasonal LHF fields are calculated. First, the LHF is calculated based on the sum of all the three components (which is approximately equal to the total field) for both the wind and humidity fields. The so-calculated LHF is then filtered into a 20–90-day band. Figure 10a shows the standard deviations of the 20–90-day filtered LHF field. The standard deviation may reflect the strength of the total intraseasonal LHF field. Note that large variabilities occur over the tropical Indian Ocean and western Pacific.

Second, the LHF is calculated based on the sum of only the background mean state and the synoptic-scale component without involving the ISO component. The same 20–90-day filter is applied to this newly calculated LHF field. Figure 10b shows the standard deviation of the 20–90-day filtered LHF field. Note that this LHF field reflects the nonlinear rectification because of the SSV-mean flow interaction. This nonlinearly rectified LHF has strong variabilities over the equatorial Indian Ocean, Bay of Bengal, South China Sea, and western and eastern North Pacific.

By comparing the standard deviation of both the intraseasonal LHF fields, one may reveal what percentage of the intraseasonal LHF comes from the SSV-mean flow interaction. Figure 11 shows the ratio of the standard deviation of the two intraseasonal LHF fields. Note that the ratio exceeds 20%–30% over the tropical Indian Ocean, western Pacific, and eastern North Pacific, indicating that over these regions, the intraseasonal surface latent heat flux is greatly modulated by the synoptic-scale motion. Maximum synoptic contributions may exceed 50% in the western and northeastern Pacific. In general,

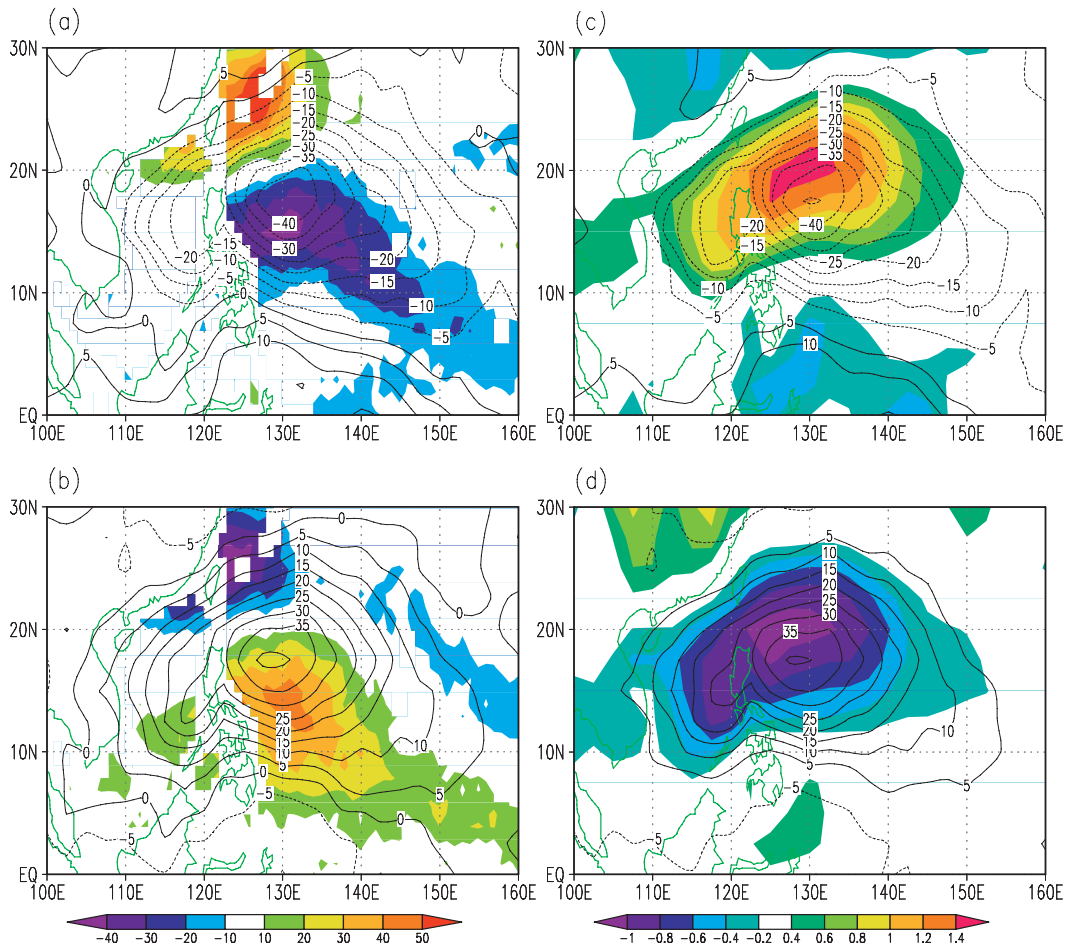


FIG. 12. (left) Spatial phase relationship between the nonlinearly rectified intraseasonal surface LHF (shading, $W m^{-2}$) and the 20–90-day filtered OLR field (contour, $W m^{-2}$) at day 0 during the (top) enhanced and (bottom) suppressed ISO phases in the NWP. (right) As in (left), but the shading is for the 20–90-day filtered specific humidity field at 925 hPa ($g kg^{-1}$). Day 0 corresponds to a time when the OLR attains a maximum or minimum value at 15° – 20° N, 125° – 135° E.

the strong nonlinear rectification appears in the region where the ISO variability is large.

What is the relative role of the synoptic-scale wind versus synoptic-scale air–sea humidity difference? A further diagnosis reveals that the synoptic-scale wind is more important in contributing to this upscale feedback when the background annual mean state is applied. With an annual cycle background state, both the synoptic-scale wind and the synoptic-scale humidity difference fields may contribute to the nonlinear rectification of LHF.

b. Phase relation between the nonlinearly rectified LHF and the ISO convection

In the previous section, we show the overall ratio of the intraseasonal LHF contributed by SSV due to the nonlinear rectification. In this section we further examine the spatial phase relationship between the nonlinearly

rectified LHF and the ISO convection/moisture. Here we focus on three major ISO convective activity regions in boreal summer: the northwestern Pacific, the tropical Indian Ocean, and the northeastern Pacific.

For the northwestern Pacific region, the same reference box (15° – 20° N, 125° – 135° E) is used to determine ISO enhanced and suppressed phases. Also, the same analysis procedure is applied to calculate the intraseasonal LHF based on the synoptic-scale and the summer mean fields. Figure 12 shows the spatial phase relation between the nonlinearly rectified LHF (shadings) and the ISO convection represented by the OLR field during the enhanced and suppressed ISO phases. Note that during the ISO wet phase, enhanced surface LHF appears at and to the northwest of the ISO convection center, while suppressed LHF is observed to the southeast of the convection center. A similar phase relation, but

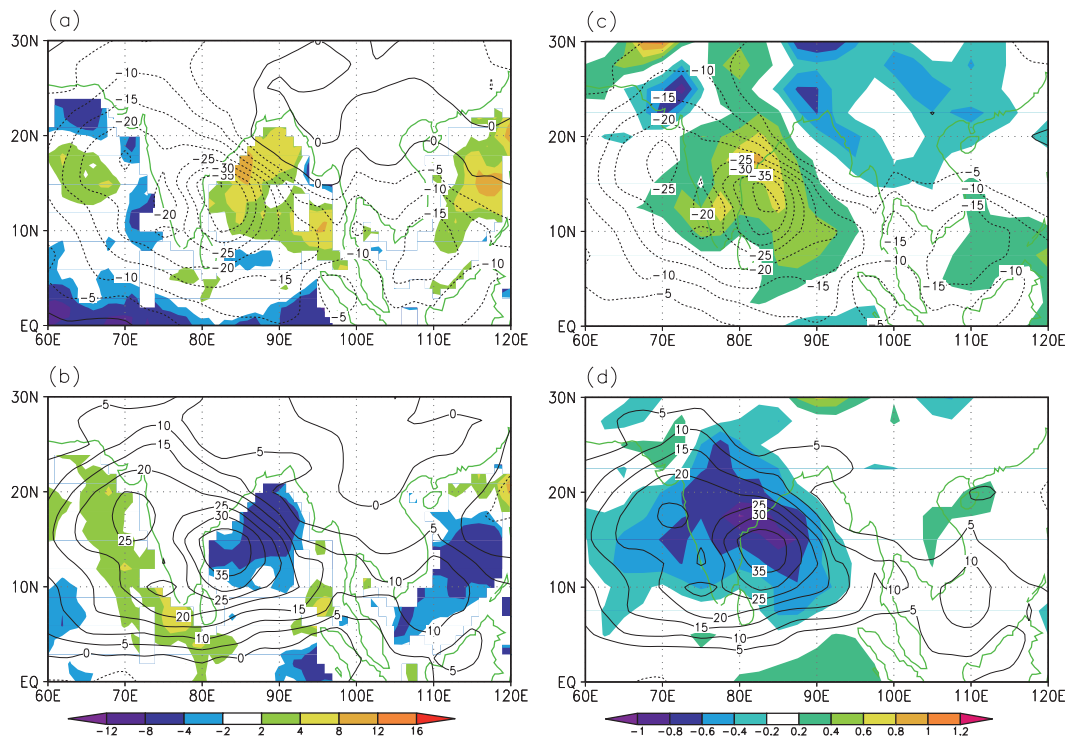


FIG. 13. As in Fig. 12, but for the tropical Indian Ocean region. The reference box for the OLR is at 10°–15°N, 80°–85°E.

with an opposite sign, appears during the ISO dry phase. The amplitude of the nonlinearly rectified LHF is quite large, exceeding 40 W m^{-2} .

What is the role of the nonlinearly rectified LHF in the ISO evolution? It is speculated that the enhanced surface LHF to the northwest of the convection due to the SSV-mean flow interaction may lead to the increase of surface moisture and convective instability in situ, and thus contribute to the strengthening and the northwestward propagation of the ISO.

To examine whether the boundary layer moisture associated with the ISO is ahead of the convection, we plot the specific humidity field at 925 hPa in Figs. 12c,d. The contribution of the nonlinearly rectified LHF to the ISO moisture field is supported by the observational evidence. A positive (negative) intraseasonal specific humidity anomaly is indeed located northwest of the ISO enhanced (suppressed) convection center, in accordance with the rectified LHF field. This suggests that the nonlinearly rectified surface LHF may play an active role in preconditioning the moisture ahead of the ISO convection center, contributing to the northwestward propagation of the ISO.

What is the ISO contribution to the intraseasonal surface LHF? To compare the ISO and SSV contributions, we calculated the surface LHF due to the ISO-mean flow

interaction (without the involvement of SSV) for the enhanced and suppressed ISO phases, respectively (figure not shown). It is found that enhanced (suppressed) surface LHF appears both north and south of the ISO convection center. Therefore, this part of the LHF does not contribute to the asymmetry of the near-surface moisture and thus has little effect on the northwestward propagation of the ISO in the WNP.

The ISO convective activity in the tropical Indian Ocean is characterized by a large-scale northwest–southeast-tilted rainband that propagates northeastward (Waliser et al. 2001; Jiang et al. 2004; Jiang and Li 2005; Wang et al. 2005). How does SSV contribute to the intraseasonal LHF in the region? Figure 13 illustrates the spatial phase relationships among the ISO convection (represented by OLR, contour), the nonlinearly rectified LHF (shading in the left panels of Fig. 13), and the intraseasonal humidity field (shading in the right panels of Fig. 13). A similar spatial structure is found in the tropical Indian Ocean region; that is, the enhanced (suppressed) nonlinearly rectified surface LHF and the positive (negative) boundary layer moisture perturbation lead the ISO-enhanced (suppressed) convection. Thus, the asymmetric SSV-induced nonlinearly rectified LHF may contribute to the asymmetry of the near-surface specific humidity, which may further contribute to the northeastward

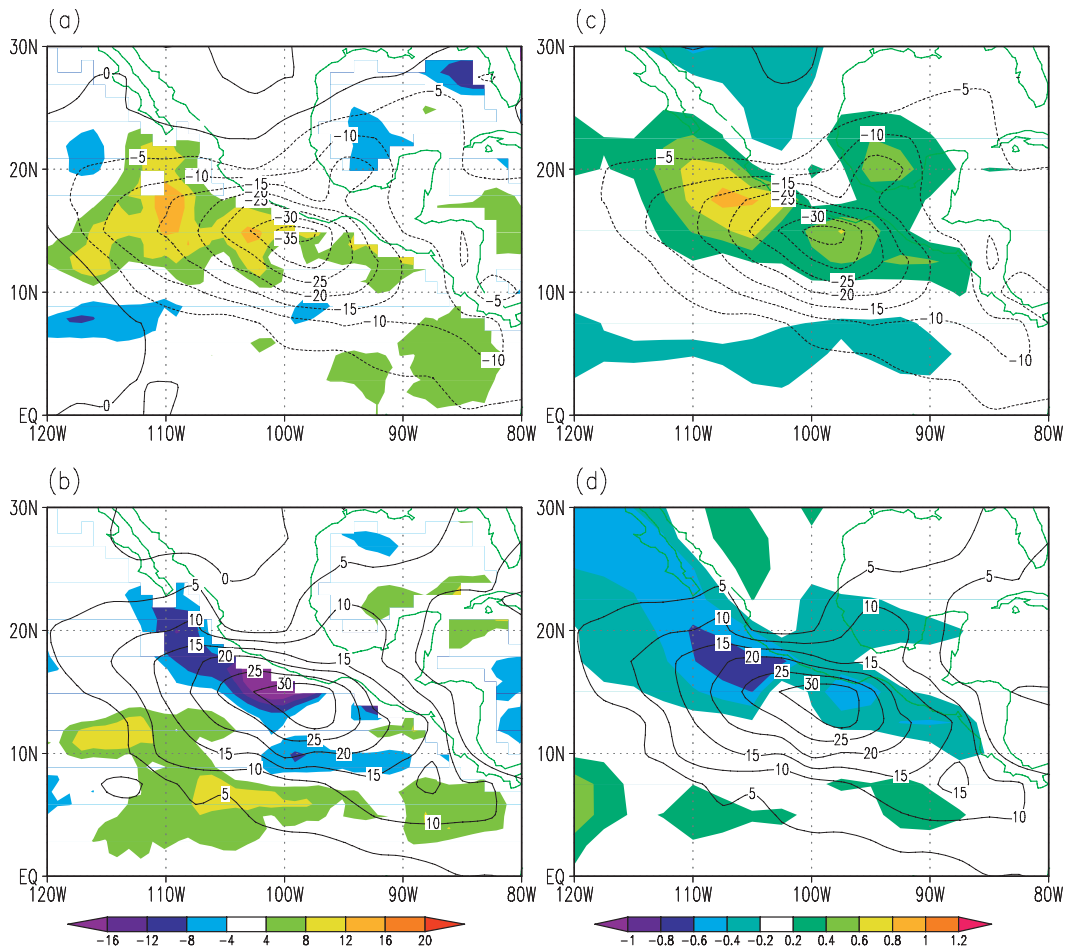


FIG. 14. As in Fig. 12, but for the northeastern Pacific region. The reference box for the OLR is at 12.5° – 15° N, 100° – 97.5° W.

propagation of ISO in boreal summer over the tropical Indian Ocean.

In boreal summer, a marked northward propagation of the intraseasonal OLR field is found in the northeastern Pacific (Jiang and Waliser 2008). To examine the nonlinear rectification effect in the region, we performed a similar calculation by selecting a reference box (12.5° – 15° N, 100° – 97.5° W) where the strongest local ISO convective activity appears. Figure 14 illustrates the spatial phase relationships among the nonlinearly rectified surface LHF, the intraseasonal specific humidity field, and the ISO convection. Similar characteristics are revealed in the northeastern Pacific, where the SSV-induced nonlinearly rectified surface LHF may contribute to the asymmetry of the PBL moisture and the northward propagation of the ISO convection.

The earlier-mentioned analyses in the three active ISO regions all point out a similar feature—that the nonlinearly rectified surface LHF leads the ISO convection center and may contribute to the asymmetry

of the near-surface moisture. This indicates that the synoptic-scale motion, through its nonlinear rectification of the surface LHF, may exert an upscale feedback to the ISO.

5. Summary

Two-way interactions between the ISO and SSV are examined based on the analysis of the observational data. It is found that the synoptic-scale (3–8 days) disturbances tend to be enhanced (weakened) during the enhanced (suppressed) ISO phase. Such an ISO-phase-dependent feature appears not only in the dynamic fields, such as 850-hPa wind and vorticity, but also in thermodynamic variables, such as the sea surface temperature and humidity fields. During the enhanced ISO phase, the northwest–southeast-oriented synoptic wave train is strong and well organized in the northwestern Pacific, while it becomes much weaker and loosely organized during the suppressed ISO phase. The mechanism for

the enhancement of the synoptic wave train during the enhanced phase is attributed to the strengthening of the background easterly shear, which favors the enhancement of the lower-tropospheric perturbations.

A bulk formula is used to calculate the contribution of the synoptic-scale motion to the intraseasonal surface latent heat flux. The ratio of the intraseasonal LHF calculated based on the sum of the synoptic-scale field and the annual mean field and based on the total fields shows that SSV contributes a significant portion of the total intraseasonal LHF in most of the tropical oceans. The maximum contributions to the intraseasonal latent heat flux by the synoptic-scale motion exceed 20%–30% over the tropical Indian Ocean, South China Sea, WNP, and northeastern Pacific. For the annual mean basic state, the major contribution comes from the synoptic wind field. The synoptic wind and humidity fields become equally important when an annual cycle basic state is considered.

A further diagnosis of the spatial phase relationship between the SSV-induced nonlinearly rectified LHF and the ISO convection in the WNP in boreal summer reveals that the LHF has maximum values to the northwest of the enhanced ISO convection center, in accordance with a positive near-surface humidity perturbation. This observational fact points out a possible upscale feedback from SSV to the ISO—that is, enhanced nonlinearly rectified LHF may increase the surface moisture and thus the atmospheric convective instability ahead of the ISO convection center, leading to the northwestward propagation of the ISO in the WNP. A similar phase leading feature is found in the tropical Indian Ocean and the northeastern Pacific, supporting the notion that SSV, whose strength is to a large extent controlled by the ISO, may exert an upscale feedback to the ISO through the nonlinear rectification of the surface LHF. Such a feedback may favor the growth and propagation of the ISO convection through the preconditioning of the surface moisture.

In this study, we focus on the upscale feedback through the modulation of the surface latent heat flux. In addition, SSV may feed back to the ISO through the atmospheric eddy momentum/energy transport and through the change of SST. Further works need to explore the additional possible processes. As the first step, we used the climatological mean state and did not consider the interannually varying basic state. It would be interesting to reveal ENSO-phase-dependent nonlinear rectification features. It is also worth mentioning that TRMM SST data might contain some errors induced by local atmospheric convection and therefore caution is needed in interpreting the SST signal associated with the synoptic-scale waves.

Acknowledgments. This work was supported by ONR Grant N000140810256 and NRL Grant N00173091G008 and by the International Pacific Research Center, which is sponsored by the Japan Agency for Marine-Earth Science and Technology (JAMSTEC), NASA (Grant NNX07AG53G), and NOAA (Grant NA17RJ1230).

REFERENCES

- Batstone, C. P., A. J. Matthews, and D. P. Stevens, 2005: Coupled ocean–atmosphere interactions between the Madden–Julian oscillation and synoptic-scale variability over the warm pool. *J. Climate*, **18**, 2004–2020.
- Biello, J. A., and A. J. Majda, 2005: A new multiscale model for the Madden–Julian oscillation. *J. Atmos. Sci.*, **62**, 1694–1721.
- , —, and M. W. Moncrieff, 2007: Meridional momentum flux and superrotation in the multiscale IPESD MJO model. *J. Atmos. Sci.*, **64**, 1636–1651.
- Chu, P. S., and J. Frederick, 1990: Westerly wind bursts and surface heat flux in the equatorial western Pacific in May 1992. *J. Meteor. Soc. Japan*, **68**, 523–537.
- Dickinson, M., and J. Molinari, 2002: Mixed Rossby–gravity waves and western Pacific tropical cyclogenesis. Part I: Synoptic evolution. *J. Atmos. Sci.*, **59**, 2183–2196.
- Frank, W. M., and P. E. Roundy, 2006: The role of tropical waves in tropical cyclogenesis. *Mon. Wea. Rev.*, **134**, 2397–2417.
- Fu, B., T. Li, M. S. Peng, and F. Weng, 2007: Analysis of tropical cyclogenesis in the western North Pacific for 2000 and 2001. *Wea. Forecasting*, **22**, 763–780.
- Ge, X., T. Li, and X. Zhou, 2007: Tropical cyclone energy dispersion under vertical shears. *Geophys. Res. Lett.*, **34**, L23807, doi:10.1029/2007GL031867.
- Hartmann, D. L., and E. D. Maloney, 2001: The Madden–Julian oscillation, barotropic dynamics, and North Pacific tropical cyclone formation. Part II: Stochastic barotropic modeling. *J. Atmos. Sci.*, **58**, 2559–2570.
- Hendon, H. H., and B. Liebmann, 1994: Organization of convection within the Madden–Julian oscillation. *J. Geophys. Res.*, **99**, 8073–8083.
- Hsu, H. H., and C. H. Weng, 2001: Northwestward propagation of the intraseasonal oscillation in the western North Pacific during the boreal summer: Structure and mechanism. *J. Climate*, **14**, 3834–3850.
- , C. H. Hung, A. K. Lo, C. C. Wu, and C. W. Hung, 2008: Influence of tropical cyclones on the estimation of climate variability in the tropical western North Pacific. *J. Climate*, **21**, 2960–2975.
- Jiang, X., and T. Li, 2005: Reinitiation of the boreal summer intraseasonal oscillation in the tropical Indian Ocean. *J. Climate*, **18**, 3777–3795.
- , and D. E. Waliser, 2008: Northward propagation of the subseasonal variability over the eastern Pacific warm pool. *Geophys. Res. Lett.*, **35**, L09814, doi:10.1029/2008GL033723.
- , T. Li, and B. Wang, 2004: Structures and mechanisms of the northward propagating boreal summer intraseasonal oscillation. *J. Climate*, **17**, 1022–1039.
- Kiladis, G. N., M. C. Wheeler, P. T. Haertel, K. H. Straub, and P. E. Roundy, 2009: Convectively coupled equatorial waves. *Rev. Geophys.*, **47**, RG2003, doi:10.1029/2008RG000266.
- Ko, K. C., and H. H. Hsu, 2009: ISO modulation on the submonthly wave pattern and recurving tropical cyclones in the tropical western North Pacific. *J. Climate*, **22**, 582–599.

- Krishnamurti, T. N., D. R. Chakraborty, N. Cubukcu, L. Stefanova, and T. S. V. Kumar, 2003: A mechanism of the MJO based on interactions in the frequency domain. *Quart. J. Roy. Meteor. Soc.*, **129**, 2559–2590.
- Lau, K.-H., and N.-C. Lau, 1990: Observed structure and propagation characteristics of tropical summertime synoptic scale disturbances. *Mon. Wea. Rev.*, **118**, 1888–1913.
- Li, T., 2006: Origin of the summertime synoptic-scale wave train in the western North Pacific. *J. Atmos. Sci.*, **63**, 1093–1102.
- , and B. Wang, 2005: A review on the western North Pacific monsoon: Synoptic-to-interannual variabilities. *Terr. Atmos. Oceanic Sci.*, **16**, 285–314.
- , B. Fu, X. Ge, B. Wang, and M. Peng, 2003: Satellite data analysis and numerical simulation of tropical cyclone formation. *Geophys. Res. Lett.*, **30**, 2122, doi:10.1029/2003GL018556.
- Liebmann, B., H. H. Hendon, and J. D. Glick, 1994: The relationship between tropical cyclones of the Western Pacific and Indian oceans and the Madden-Julian oscillation. *J. Meteor. Soc. Japan*, **72**, 401–412.
- Lin, A., and T. Li, 2008: Energy spectrum characteristics of boreal summer intraseasonal oscillations: Climatology and variations during the ENSO developing and decaying phases. *J. Climate*, **21**, 6304–6320.
- Lindzen, R. S., and S. Nigam, 1987: On the role of sea surface temperature gradients in forcing low-level winds and convergence in the tropics. *J. Atmos. Sci.*, **44**, 2418–2436.
- Madden, R. A., and P. R. Julian, 1971: Detection of a 40–50 day oscillation in the zonal wind in the tropical Pacific. *J. Atmos. Sci.*, **28**, 702–708.
- , and —, 1972: Description of global-scale circulation cells in the tropics with a 40–50 day period. *J. Atmos. Sci.*, **29**, 1109–1123.
- , and —, 1994: Observations of the 40–50-day tropical oscillation—A review. *Mon. Wea. Rev.*, **122**, 814–837.
- Maloney, E. D., and D. L. Hartmann, 1998: Frictional moisture convergence in a composite life cycle of the Madden-Julian oscillation. *J. Climate*, **11**, 2387–2403.
- , and —, 2000a: Modulation of eastern North Pacific hurricanes by the Madden-Julian oscillation. *J. Climate*, **13**, 1451–1460.
- , and —, 2000b: Modulation of hurricane activity in the Gulf of Mexico by the Madden-Julian Oscillation. *Science*, **287**, 2002–2004.
- , and —, 2001: The Madden-Julian oscillation, barotropic dynamics, and North Pacific tropical cyclone formation. Part I: Observations. *J. Atmos. Sci.*, **58**, 2545–2558.
- , and M. J. Dickinson, 2003: The intraseasonal oscillation and the energetics of summertime tropical western North Pacific synoptic-scale disturbances. *J. Atmos. Sci.*, **60**, 2153–2168.
- Nakazawa, T., 1988: Tropical super clusters within intraseasonal variations over the western Pacific. *J. Meteor. Soc. Japan*, **66**, 823–839.
- Roundy, P. E., and J. R. Kravitz, 2009: The association of the evolution of intraseasonal oscillations to ENSO phase. *J. Climate*, **22**, 381–395.
- Rui, H., and B. Wang, 1990: Development characteristics and dynamic structure of tropical intraseasonal convection anomalies. *J. Atmos. Sci.*, **47**, 357–379.
- Seiki, A., Y. N. Takayabu, K. Yoneyama, N. Sato, and M. Yoshizaki, 2009: The Oceanic Response to the Madden-Julian Oscillation and ENSO. *Sci. Online Lett. Atmos.*, **5**, 93–96.
- Sobel, A. H., and E. D. Maloney, 2000: Effect of ENSO and the MJO on western North Pacific tropical cyclones. *Geophys. Res. Lett.*, **27**, 1739–1742.
- Straub, K. H., and G. N. Kiladis, 2003: Interactions between the boreal summer intraseasonal oscillation and higher-frequency tropical wave activity. *Mon. Wea. Rev.*, **131**, 945–960.
- Tam, C.-Y., and T. Li, 2006: The origin and dispersion characteristics of the observed summertime synoptic-scale waves over the western Pacific. *Mon. Wea. Rev.*, **134**, 1630–1646.
- Waliser, D. E., Z. Zhang, K. M. Lau, and J. H. Kim, 2001: Interannual sea surface temperature variability and the predictability of tropical intraseasonal variability. *J. Atmos. Sci.*, **58**, 2596–2615.
- Wang, B., and X. Xie, 1996: Low-frequency equatorial waves in vertically shear flow. Part I: Stable waves. *J. Atmos. Sci.*, **53**, 449–467.
- , P. J. Webster, and H. Teng, 2005: Antecedents and self-induction of active-break south Asian monsoon unraveled by satellites. *Geophys. Res. Lett.*, **32**, L04704, doi:10.1029/2004GL020996.
- Weare, B. C., P. T. Strub, and M. D. Samuel, 1981: Annual mean surface heat fluxes in the tropical Pacific Ocean. *J. Phys. Oceanogr.*, **11**, 705–717.
- Yasunari, T., 1979: Cloudiness fluctuations associated with the Northern Hemisphere summer monsoon. *J. Meteor. Soc. Japan*, **57**, 227–242.
- Yu, L., and R. A. Weller, 2007: Objectively analyzed air–sea heat fluxes for the global ice-free oceans (1981–2005). *Bull. Amer. Meteor. Soc.*, **88**, 527–539.
- Zhang, C., 2005: Madden-Julian Oscillation. *Rev. Geophys.*, **43**, RG2003, doi:10.1029/2004RG000158.